DISCOVERY OF A HIGHLY ENERGETIC PULSAR ASSOCIATED WITH IGR J14003−6326 IN THE YOUNG UNCATALOGED GALACTIC SUPERNOVA REMNANT G310.6−1.6

M. Renaud[1,2], V. Marandon[1], E. V. Gotthelf[3], J. Rodriguez[4], R. Terrier[1], F. Mattana[1], F. Lebrun[1], J. A. Tomsick[5], and R. N. Manchester[6]

[1] AstroParticule et Cosmologie (APC), CNRS-UMR 7164, Université Paris 7 Denis Diderot, F-75205 Paris, France; mrenaud@lpta.in2p3.fr
[2] Laboratoire de Physique Théorique et Astroparticules (LPTA), CNRS-UMR 5207, Université Montpellier II, F-34095 Montpellier, France
[3] Columbia Astrophysics Laboratory, Columbia University, 550 West 120th Street, New York, NY 10027, USA
[4] CEA Saclay, Laboratoire AIM, CNRS-UMR 7158, DSM/IRFU/Service d'Astrophysique, F-91191 Gif-sur-Yvette, France
[5] Space Sciences Laboratory, 7 Gauss Way, University of California, Berkeley, CA 94720-7450, USA
[6] CSIRO Astronomy and Space Science, Australia Telescope National Facility, P.O. Box 76, Epping NSW 1710, Australia

ABSTRACT

We report the discovery of 31.18 ms pulsations from the *INTEGRAL* source IGR J14003−6326 using the *Rossi X-ray Timing Explorer* (*RXTE*). This pulsar is most likely associated with the bright *Chandra* X-ray point source lying at the center of G310.6−1.6, a previously unrecognized Galactic composite supernova remnant (SNR) with a bright central non-thermal radio and X-ray nebula, taken to be the pulsar wind nebula (PWN). PSR J1400−6325 is amongst the most energetic rotation-powered pulsars in the Galaxy, with a spin-down luminosity of $\dot{E} = 5.1 \times 10^{37}$ erg s^{-1}. In the rotating dipole model, the surface dipole magnetic field strength is $B_s = 1.1 \times 10^{12}$ G and the characteristic age $\tau_c \equiv P/2\dot{P} = 12.7$ kyr. The high spin-down power is consistent with the hard spectral indices of the pulsar and the nebula of 1.22 ± 0.15 and 1.83 ± 0.08, respectively, and a 2–10 keV flux ratio $F_{\mathrm{PWN}}/F_{\mathrm{PSR}} \sim 8$. Follow-up Parkes observations resulted in the detection of radio emission at 10 and 20 cm from PSR J1400−6325 at a dispersion measure of ∼560 cm^{-3} pc, which implies a relatively large distance of 10 ± 3 kpc. However, the resulting location off the Galactic plane of ∼280 pc would be much larger than the typical thickness of the molecular disk, and we argue that G310.6−1.6 lies at a distance of ∼7 kpc. There is no gamma-ray counterpart to the nebula or pulsar in the *Fermi* data published so far. A multi-wavelength study of this new composite SNR, from radio to very high-energy gamma rays, suggests a young ($\lesssim 10^3$ yr) system formed by a sub-energetic ($\lesssim 10^{50}$ erg), low ejecta mass ($M_{\mathrm{ej}} \sim 3\,M_\odot$) supernova explosion that occurred in a low-density environment ($n_0 \sim 0.01$ cm^{-3}).

Key words: gamma rays: general – pulsars: individual (PSR J1400-6325) – ISM: supernova remnants – X-rays: individual (IGR J14003-6326, G310.6-1.6)

Online-only material: color figure

1. INTRODUCTION

The number of known supernova remnants (SNRs) in the Galaxy has increased significantly over the last few years, mainly due to a new generation of radio and X-ray instruments of unprecedented sensitivities and angular resolutions. In particular, these observations, combined with Galactic Plane Surveys (e.g., Brogan et al. 2006), and targeted observations (e.g., Gelfand & Gaensler 2007; Gaensler et al. 2008) have increased the fraction of SNRs found to harbor an energetic pulsar powering a wind nebula (the so-called composite SNRs). Moreover, deep observations toward compact pulsar wind nebulae (PWNe) have proven to be successful in detecting their powering pulsars (Camilo et al. 2009; Gotthelf & Halpern 2009), providing constraints on their energetics, spin evolution, and birth parameters. Along with the current generation of high/very high energy (VHE; >100 GeV) instruments, these observations are of prime importance for understanding the structure and evolution of these sources, and the underlying acceleration mechanisms which occur close to the pulsar, and at the relativistic and non-relativistic shock fronts bounding the PWN and the host SNR (Gaensler & Slane 2006).

The soft γ-ray source IGR J14003−6326 was discovered in a deep *INTEGRAL*/IBIS/ISGRI mosaic of the Circinus region as a persistent source at the mCrab level (Keek et al. 2006). A *Swift*/XRT survey of *INTEGRAL* sources located IGR J14003−6326 to 4″ in 2–10 keV X-rays, but no conclusion was reached on

its nature (Malizia et al. 2007). A follow-up *Chandra* survey of unidentified IGR sources reported a PWN within a ∼3′ diameter nearly circular emission nebula (Tomsick et al. 2009). These authors presented the 0.3–10 keV spectrum of the total emission by an absorbed power law with a relatively hard photon index ($\Gamma = 1.82 \pm 0.13$) and a large column density $N_{\mathrm{H}} \sim 3 \times 10^{22}$ cm^{-2}.

In this paper, we report the discovery with the *Rossi X-ray Timing Explorer* (*RXTE*) of 31.18 ms pulsations toward IGR J14003−6326, and the radio detection in follow-up observations using the Parkes telescope. We present a multi-wavelength study of this new Galactic composite SNR, G310.6−1.6, using radio, X-ray, and gamma-ray data. PSR J1400−6325 is one of the most energetic in the Galaxy and powers a wind nebula whose broadband non-thermal synchrotron emission is measured in radio and X-rays. We present a spatial and spectral analysis that shows evidence for a young SNR, formed from a sub-energetic, low ejecta mass supernova (SN) explosion that occurred in a low-density environment. We also discuss the implications of the lack of high-energy (HE) gamma-ray emission in the *Fermi* data.

2. OBSERVATIONS AND RESULTS

2.1. Chandra

We have performed a re-analysis of the *Chandra* data of the IGR J14003−6326 field (Tomsick et al. 2009) taken on
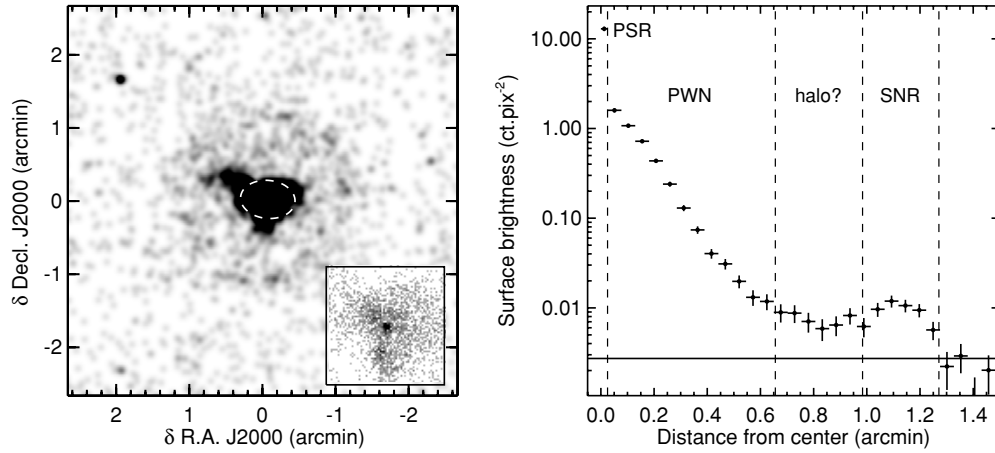
Figure 1. Left: *Chandra*/ACIS-I count rate image of G310.6−1.6 in the 0.5–10 keV energy range, smoothed with a Gaussian of $\sigma = 5''$ (linear scale). The dashed ellipse shows the intrinsic size of the radio MGPS-2 extended source cataloged at 843 MHz (Murphy et al. 2007; see Section 2.5). The bright, central, point-like source is better revealed in the inset unsmoothed image of the central regions of the SNR. Right: surface brightness profile of the *Chandra*/ACIS emission, centered on the point-like source. The background level is depicted by the horizontal solid line. The dashed lines delineate the regions of interest, namely the PSR, the PWN, the putative X-ray halo, and the host SNR.

2008 June 29 UT, using the Advanced CCD Imaging Spectrometer (ACIS; Garmire et al. 2003) and operating in TIME/FAINT exposure mode. The live time amounts to 5077 s, corrected from the 1.3% readout dead time. The maximum pixel count rate within the source is 0.015 counts s^{-1}, so pile-up effect could be safely ignored. All the data reduction and analysis were performed with the *Chandra* Interactive Analysis of Observation software (CIAO) version 4.1.2, using the CALibration DataBase (CALDB) v4.1.3. Figure 1 (left) shows the 0.5–10 keV *Chandra* image centered on IGR J14003−6326, which exhibits a characteristic morphology of a composite SNR, as revealed by the radial profile of the surface brightness (Figure 1, right). In particular, the excess emission at $1'.1$–$1'.2$ from the center is found to be the clear signature of the host shell-type SNR. We have considered three regions of interest, namely the bright point-like source (PSR), the diffuse surrounding emission (PWN), and the shell-like structure (SNR). As shown on the profile, some faint emission seems to extend up to the shell-type structure, at distances of ∼$1'$ from the PSR. In view of the large N_H, this could be partly explained by a dust-scattering halo, similar to those observed in other PWNe, such as G21.5-0.9 (Slane et al. 2000; Safi-Harb et al. 2001; Bocchino et al. 2005). Unfortunately, the lack of statistics prevents us from drawing any firm conclusion about the nature of this extended X-ray emission. The source-free region used to extract the background was taken on the same CCD chip as the source, in a circle of $1'.45$ in radius. Apart from the PWN emission, the low count levels led us to fit the three components simultaneously, with a common hydrogen column density $N_H = (2.09 \pm 0.12) \times 10^{22}$ cm^{-2}. As noticed by Tomsick et al. (2009), this value is of the same order as the Galactic value,[7] and suggests a large distance and/or local absorption.

The best-fit position of the point-like source is R.A.(J2000) $= 14^h00^m45^s.69$, decl.(J2000) $= -63°25'42''.6$ (Tomsick et al. 2009). For the spectral analysis, we chose an integration region of $1''.5$ in radius centered on the source and estimated the source background using counts extracted from a concentric annulus of radii $1''.5$ and $2''$. Fits to the background subtracted spectrum are

not tightly constrained, even though a power law gives slightly better results than any thermal model. The spectrum is hard, with a best-fit power-law index of 1.22 ± 0.15 and an unabsorbed 2–10 keV flux of $(1.95 \pm 0.5) \times 10^{-12}$ erg cm^{-2} s^{-1}. The PWN integration region was taken in an annulus centered on the PSR position, with an inner radius of $1''.5$ and an outer radius of $0'.65$ (see Figure 1, right). The best-fit power-law index and the unabsorbed 2–10 keV flux are found to be 1.83 ± 0.09 and $(1.51 \pm 0.20) \times 10^{-11}$ erg cm^{-2} s^{-1}, respectively. Therefore, the PWN is by far the dominant component in X-rays and these spectral results are in close agreement with those obtained by Tomsick et al. (2009) on the total emission. The SNR integration region was defined as an annulus, with inner and outer radii of 0.98 and $1'.27$, respectively. As for the PSR, due to the low statistics, the SNR spectrum is rather poorly constrained and does not allow us to clearly distinguish between thermal and power-law models, although no strong X-ray lines are present. A power-law fit gives a rather soft spectrum, with a best-fit spectral index of 2.56 ± 0.18 and an unabsorbed 2–10 keV flux of $(1.0 \pm 0.2) \times 10^{-12}$ erg cm^{-2} s^{-1}. Whatever is the nature of the X-ray emission, the flux measured with *Chandra* can be considered as an upper limit on the synchrotron emission. We then converted the best-fit power-law spectrum to a surface brightness at 4 keV of ∼5×10^{32} erg pc^{-2} s^{-1} sr^{-1}, as this will be compared to theoretical predictions in Section 3.

2.2. RXTE

The X-ray flux measured from the *Chandra* point source in G310.6−1.6 is sufficient to search for the expected pulsations using *RXTE*. A pair of 44 ks exposures were obtained a year apart on 2008 September 29 UT and 2009 September 30. Data were collected with the Proportional Counter Array (PCA; Jahoda et al. 1996) in the GoodXenon mode with an average of 1.5 and 2.2 out of the five proportional counter units (PCUs) active, for the two observations, respectively. In this mode, photons are time-tagged to 0.9 μs and have an absolute uncertainty better than 100 μs. The effective area of five combined units is 6500 cm^2 at 10 keV with a roughly circular field of view of ∼$1°$ FWHM. Spectral information is available in the 2–60 keV energy band with a resolution of ∼16% at 6 keV. The standard time filters were applied to the PCA data, which rejects intervals

---

[7] We make use here of the Anders & Grevesse (1989) abundances, rather those of Wilms et al. (2000), as done in Tomsick et al. (2009). Using the latter abundances yields compatible $N_H \sim 3 \times 10^{22}$ cm^{-2}.
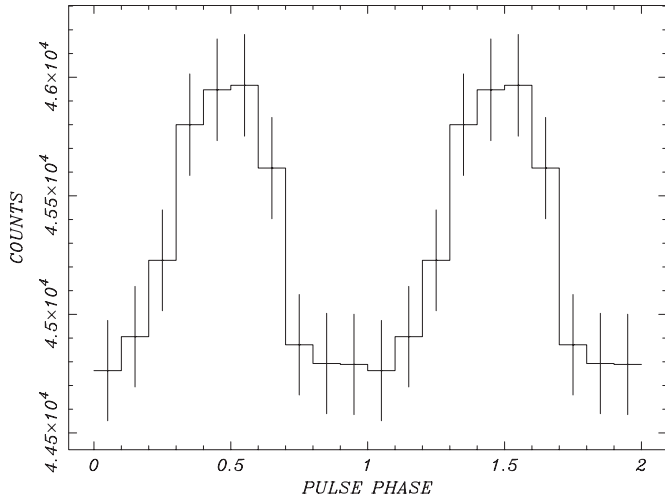
Figure 2. PSR J1400−6325 folded light curve in the *RXTE* PCA 2–20 keV band. Two cycles are shown for clarity. Phase zero is arbitrary.

Table 1
Measured and Derived Parameters for PSR J1400−6325

Parameter	Value
R.A. (J2000)....	$14^{\rm h}00^{\rm m}45\overset{s}{.}69$
Decl. (J2000)....	$-63°25'42\overset{''}{.}6$
Period, P_1 (ms) at MJD 54738....	31.180373(2)
Period, P_2 (ms) at MJD 55105....	31.1816011(3)
Period derivative, $\dot{P}$....	$3.890(6) \times 10^{-14}$
Dispersion measure (cm^{-3} pc)....	563 ± 4
Flux density at 10 cm (μJy)....	$\sim$110
Flux density at 20 cm (μJy)....	$\sim$250
Flux density at 50 cm (μJy)....	< 500
Characteristic age, τ_c (kyr)....	12.7
Spin-down luminosity, $\dot{E}$ (erg s^{-1})....	5.1×10^{37}
Surface dipole magnetic field, B_s (G)....	1.1×10^{12}
DM-based distance (kpc)....	10 ± 3

Note. 1σ uncertainties given.

of South Atlantic Anomaly passages, Earth occultations, and other periods of high particle activity. The photon arrival times were transformed to the solar system barycenter in Barycentric Dynamical Time (TDB) using the JPL DE200 ephemeris and the *Chandra* coordinates for the point source.

2.2.1. Timing Analysis

We restricted the *RXTE* timing analysis to photon data with energies in the 2–20 keV range (PCA channels 2–50) recorded in the top Xenon layer of each PCU, to optimize the signal-to-noise ratio (S/N). For the first observation, we further excluded one 4 ks non-contiguous data segment at the beginning of the run, resulting in 33.4 ks of filtered time spanning 45 ks. A 2^{26} fast Fourier transform (FFT) of the data binned in 1 ms steps revealed a significant signal of power $S = 55$ at a period of $P = 31.1$ ms. For the 6.7×10^7 search elements this corresponds to a false detection probability for a blind search down to 1 ms of $\wp = 7.6 \times 10^{-5}$ (99.9924% confidence level). We refined this signal using a Z_1^2 statistics which yields a signal power $Z_1^2 = 53.76$ at a period of $P = 31.180373(2)$ ms. The 1σ uncertainty on the last digit is given in parentheses. Figure 2 displays the pulse profile in the 2–20 keV band folded at this period; the profile is narrower than a sinusoid, somewhat boxy, with a well delineated off-pulse region. We do not see any evidence for energy dependence of the pulse profile when subdividing the 2–20 keV band. The signal does not match any cataloged pulsar in the field of view, in particular the pulsars PSR J1403−6310 ($P = 0.39910$ s) and PSR J1401−6357 ($P = 0.84279$ s). In order to ensure that we have not picked up an aliased signal from these PSRs, the data were rebarycentered at their respective coordinates and searched for the known pulse period. No signal was detected apart from the original one reported above.

Based on a probable detection of a highly energetic PSR, we requested a second *RXTE* observation to confirm this result and determine the PSR spin-down rate. For the 2009 data, we followed the same procedures outlined above and constructed a Z_1^2 periodogram around the expected signal. This yielded a significant signal at $P = 31.1816011(3)$ ms with power $Z_1^2 = 116.28$, corresponding to a negligible probability of false detection. This result confirms the previous detection and provides a period derivative measurement of $\dot{P} = (3.890 \pm$

$0.006) \times 10^{-14}$. The 1σ error is derived from the root sum of the variance of the period uncertainties. The ephemeris is presented in Table 1 along with the inferred spin-down parameters. The derived spin-down power $\dot{E} = 4\pi^2 I \dot{P}/P^3 = 5.1 \times 10^{37} I_{45}$ erg s^{-1} (I_{45} is the moment of inertia in units of 10^{45} g cm^2) makes PSR J1400−6325 one of most energetic Galactic pulsars known, a close tie with several recently reported energetic rotation-powered pulsars (Camilo et al. 2009; Gotthelf & Halpern 2009). In the dipole pulsar model, the characteristic age $\tau_c = P/2\dot{P} = 12.7$ kyr, assuming $P \gg P_0$ (the initial PSR period), and the surface dipole magnetic field $B_s = 1.1 \times 10^{12}$ G. Based on the associated PWN and SNR, its estimated luminosity and its spin-down properties, PSR J1400−6325 is clearly a Crab-like, young energetic rotation-powered PSR responsible for the observed PWN.

The pulsed emission of PSR J1400−6325 is well isolated in phase with nearly constant emission in-between. This allowed us to take advantage of phase-resolved spectroscopy to obtain a spectrum of the pulsed flux using the off-pulse emission as a near perfect representation of the background plus unpulsed spectrum. We generated phase-resolved spectra in 20 phase bins using the *RXTE* FTOOL *fasebin*, aligning the two observations to a common phase and summing the result. From this combined spectral file, we generated on- and off-pulsed spectra as input into the XSPEC spectral fitting package. The response matrix for the phase-resolved spectra was generated using the same photon file, selecting only photons from the top layer of each PCU (LR1) to match the *fasebin* output. We divided the data in to two phases, 0.5 cycles apart to characterize the on-pulse signal and the off-pulse signal, respectively. We fitted the on-pulse spectrum with an absorbed power-law spectral model over the 2–10 keV band, outside of which the background dominated the pulsed signal. The column density was fixed to the *Chandra* value as *RXTE*, with its higher energy band, is unable to constrain this parameter. For an $N_{\rm H} = 2.09 \times 10^{22}$ cm^{-2} the best-fit photon index is $2.0^{+0.5}_{-0.3}$ with a $\chi^2 = 1.2$ for 17 degrees of freedom (see Figure 3). The measured 2–10 keV pulsed flux is 3.0×10^{-13} erg cm^{-2} s^{-1} (absorbed) and represents $\sim$18% of the total flux from the *Chandra* source.

2.2.2. Spectral Analysis

In order to extract the total *RXTE*/PCA spectrum, dominated by the PWN, we also accumulated spectra restricted to the top layer of PCU 2. The background was estimated using the faint
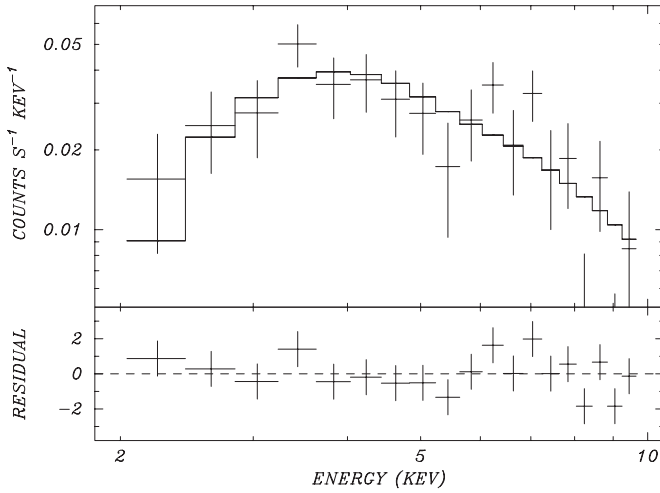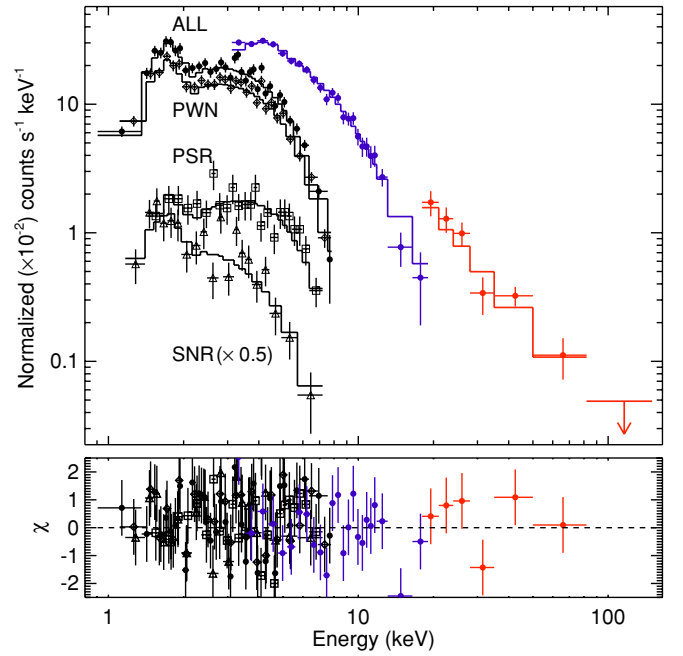
Figure 3. PSR J1400−6325 pulsed spectrum in the *RXTE* PCA 2–20 keV band fitted to an absorbed power-law model given in the text. The residuals from the best-fit model are show. The off-peak spectrum is used as background (see the text).

Figure 4. Spectra of the different components of G310.6−1.6 measured with *Chandra* (in black). The SNR spectrum was divided by 2 for sake of clarity. The *RXTE*/PCA and *INTEGRAL*/IBIS/ISGRI spectra are shown in blue and red, respectively. Solid lines represent the best-fit models (see Table 2). An absorbed power law was used to fit simultaneously the individual *Chandra* components, while an absorbed broken power law was fit to the *Chandra* spectrum of the whole X-ray emission, together with the *RXTE*/PCA and IBIS/ISGRI spectra. Residuals are shown in the lower panel.

(A color version of this figure is available in the online journal.)

model. Given the sky position of IGR J14003−6326, X-ray emission from the Galactic ridge can contribute to the PCA spectrum. Following previous works (e.g., Prat et al. 2008; Rodriguez et al. 2009), we estimated its level according to the Valinia & Marshall (1998) model, and by assuming that *Chandra* and *RXTE*/PCA are perfectly cross-calibrated. After removing the Galactic X-ray contribution, we found that a power-law fit to the 3–20 keV PCA spectrum gives an N_H similar to that found for the three *Chandra* components, though not well constrained, $(2.25 \pm 1.1) \times 10^{22}$ cm^{-2}. Freezing it to the value measured with *Chandra* leads to a spectral index of 2.19 ± 0.10 and an unabsorbed 3–20 keV flux of $(1.57 \pm 0.3) \times 10^{-11}$ erg cm^{-2} s^{-1}. The spectrum measured with PCA turns out to be softer than that measured with *Chandra*/ACIS in the 2–10 keV band. This can be explained by the presence of a break or steepening at high energies in the PWN spectrum. Thus, we also fitted the PCA spectrum with a broken power law, with N_H and a photon index before the break frozen to the *Chandra* values, and found a marginal evidence for such a break at ∼3 keV, with a photon index at higher energies of 2.21 ± 0.09, though with a slightly larger χ^2. This emission detected by *RXTE*/PCA is most likely related to G310.6−1.6, and mainly to the PWN diffuse emission, since no other significant X-ray source lies within the PCA field of view at 2° from IGR J14003−6326.

2.3. INTEGRAL IBIS/ISGRI

We analyzed all the public IBIS/ISGRI data, from revolution 46 to 713, at less than 12° from IGR J14003−6326, with the Off-Line Scientific Analysis (OSA) software (Goldwurm et al. 2003), version 7.0. After removing all the noisy pointings, as defined in Renaud et al. (2006), the total effective time amounts to ∼3.5 Ms. Mosaic images were produced in six energy bands from 18 to 65 keV with an additional band between 82 and 150 keV, in order to extract the non-thermal continuum source spectrum. Furthermore, the very small apparent size of G310.6−1.6 ($\Phi \sim 2'.3 = 4.7\, d_7$ pc, with $d = 7\, d_7$ kpc) is reminiscent of a young SNR. To search for evidence of ^{44}Ti line emission at 67.9 and 78.4 keV, expected from a young remnant, we also generated mosaic images in the 65–71, 71–75, and 75–82 keV energy bands. These lines emerge from the radioactive decay of the short-lived ^{44}Ti nucleus (with a

weighted-average lifetime of 85 ± 0.4 yr; see Ahmad et al. 2006 and references therein). Although firmly detected in only the ∼330 yr old Cas A SNR (Iyudin et al. 1994; Vink et al. 2001; Renaud et al. 2006), this radioactive element can provide invaluable constraints on the key parameters of the SN explosion.

In the 18–50 keV mosaic image, the best-fit position of IGR J14003−6326 is found to be consistent with the results obtained by Bird et al. (2007), and compatible with a point-like source coincident with G310.6−1.6. The continuum emission is safely detected with IBIS/ISGRI up to 65 keV and the spectrum is fit by a power law with a photon index of 2.33 ± 0.29 and a 20–100 keV flux of $(1.24 \pm 0.17) \times 10^{-11}$ erg cm^{-2} s^{-1}. No evidence of ^{44}Ti line emission was detected in the direction of IGR J14003−6326, and we set a 3σ upper limit of 1.5×10^{-5} ph cm^{-2} s^{-1}, after combining the two ^{44}Ti energy bands.

2.4. Spectral Properties of G310.6−1.6

Spectra of the different components measured with *Chandra*, together with those of *RXTE*/PCA and IBIS/ISGRI are shown in Figure 4, and spectral model fits are reported in Table 2. In the 2–10 keV band, the PWN accounts to ∼85% of the whole emission. A simultaneous fit on the three spectra (*Chandra* total emission, *RXTE*/PCA and IBIS/ISGRI) indicates that a broken power law is better at describing the 0.8–100 keV total emission. According to the *F*-test, this model is favored over a pure power law at the 3.5σ confidence level (probability of 2×10^{-4}). The break energy is measured at 5.6 ± 0.7 keV, and the photon index at higher energies nicely matches that measured by IBIS/ISGRI. We also performed a spectro-imaging analysis of the PWN, in order to search for any spectral softening at larger distances

Table 2
Imaging-Spectroscopy of G310.6−1.6 and PSR J1400−6325 and its Pulsar Wind Nebula

Source/Instrument	Power Law				Broken Power Law					
	N_H[a]	Γ	Flux[b]	χ^2/ν	N_H[a]	Γ_1	E_b[c]	Γ_2	Flux[b]	χ^2/ν
PSR (pulsed) *RXTE*	2.09 (–)	2.0 (0.40)	0.36 (0.2)	20.4/17	⋯	⋯	⋯	⋯	⋯	⋯
PSR (total) *Chandra*	2.09 (0.12)	1.22 (0.15)	1.95 (0.5)	182.5/191	⋯	⋯	⋯	⋯	⋯	⋯
SNR *Chandra*	2.09 (0.12)	2.56 (0.18)	1.00 (0.2)	182.5/191	⋯	⋯	⋯	⋯	⋯	⋯
PWN *Chandra*	2.09 (0.12)	1.83 (0.09)	15.1 (2.0)	182.5/191	⋯	⋯	⋯	⋯	⋯	⋯
RXTE/PCA	2.09 (–)	2.19 (0.10)	15.7 (3.0)	31.8/30	2.09 (–)	1.83 (–)	3.0 (2.0)	2.21 (0.09)	15.7 (3.5)	31.8/29
IBIS/ISGRI	⋯	2.33 (0.29)	12.4 (1.7)	7.2/7	⋯	⋯	⋯	⋯	⋯	⋯
Total[d]	2.46 (0.08)	2.16 (0.03)	13.4 (0.8)	272.6/246	2.13 (0.13)	1.90 (0.11)	5.6 (0.7)	2.30 (0.07)	10.6 (1.5)	257.1/244
PWN[e]	⋯	⋯	⋯	⋯	2.13 (0.14)	1.90 (0.10)	6.0 (0.5)	2.59 (0.11)	5.3 (0.8)	257.1/244

Notes. The uncertainties quoted are at the 68% confidence level.
[a] In units of 10^{22} cm^{-2}, assuming the Anders & Grevesse (1989) abundances
[b] 2–10 (*Chandra*), 3–20 (*RXTE*/PCA), and 20–100 keV (IBIS/ISGRI, total and PWN) unabsorbed fluxes, in units of 10^{-12} erg cm^{-2} s^{-1}.
[c] Break energy in units of keV.
[d] Total spectrum in the 0.8–100 keV energy range.
[e] PWN spectrum in the 0.8–100 keV energy range, after removing the PSR and SNR contributions.

from the PSR, as expected from efficient synchrotron burn-off of high-energy electrons accelerated in the central regions (see, e.g., Slane et al. 2000, in the case of G21.5−0.9). We fixed the N_H to the best-fit *Chandra* value and found a 2.5σ evidence of a spectral softening, from $\Gamma = 1.68 \pm 0.09$ at $5''$ from the PSR, to 2.09 ± 0.09 at the edge of the nebula. In order to measure the 0.8–100 keV PWN spectrum, we first constrained the PSR spectral index and 2–10 keV flux to be ∼1.4 and 1.7×10^{-12} erg cm^{-2} s^{-1} *at most*, in order not to violate the IBIS/ISGRI 3σ upper limit in the 82–150 keV energy range, while being still consistent with the *Chandra* values, at the 1σ confidence level. Then, we performed a second simultaneous fit on the three spectra (*Chandra* total emission, *RXTE*/PCA, and IBIS/ISGRI), by freezing the 0.8–10 keV PSR and SNR spectra to the best-fit values, and extracted the *minimum* 0.8–100 keV spectrum of the PWN, whose parameters are presented in Table 2 (last row). We find that a broken power-law fit gives a break energy of 6.0 ± 0.5 keV, in agreement with that measured above. Due to the hard PSR spectrum, assumed to extend up ∼100 keV with the same spectral index, the *minimum* PWN spectrum at higher energies is softer than the total emission, but statistically consistent with the spectrum measured by IBIS/ISGRI.

2.5. Radio

2.5.1. Pulsar

A search for a radio counterpart to the X-ray pulsar was carried out using the Parkes 64 m radio telescope of the Australia Telescope National Facility, CSIRO Astronomy and Space Science, in the 10, 20, and 50 cm bands. Observations were made with the center beam of the 20 cm multibeam receiver and analog filterbank system (Manchester et al. 2001) with sampling interval of 250 μs on 2009 October 11 (2 hr) and 2009 November 26 (4 hr), and the 10–50 cm receiver and Parkes digital filterbank systems (1 hr at each of 10 cm and 50 cm) on 2009 October 13. The received center frequencies were 3100, 1374, and 732 MHz at 10, 20, and 50 cm, respectively, and the corresponding bandwidths were 1024, 256, and 64 MHz. A search of the October data over a period range of ±60 μs about the nominal pulsar period (see Table 1) and a dispersion measure (DM) range of 0 to 1500 cm^{-3} pc yielded some possible candidates with DMs in the range 400–600 cm^{-3} pc and S/Ns of ≲6.5. A similar analysis of the 20 cm longer observation in November gave a positive detection with S/N of 8.8 at the
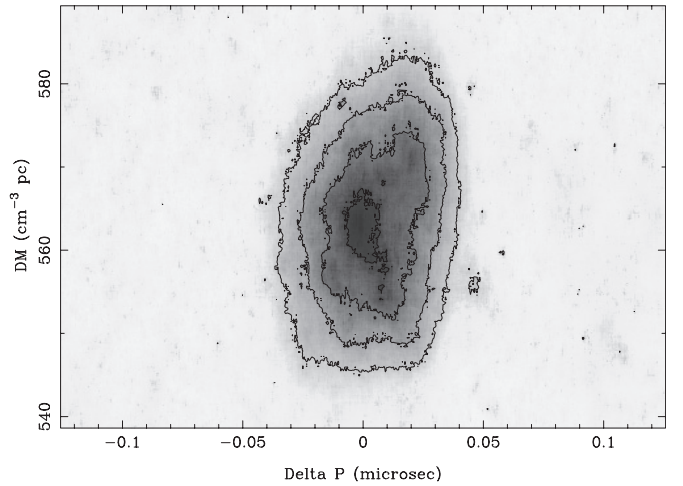
Figure 5. Plot of the 20 cm radio pulse S/N in the pulse period—DM plane around the detection values from the 2009 November Parkes observations. The gray scale is linear between S/N values of 0 and 10. S/N contours at 5, 6, 7, and 8 are overlaid.

predicted pulse period and at a DM of 563 ± 4 cm^{-3} pc, as shown in Figure 5. This detection corresponds to one of the candidates from the analysis of the October 20 cm observations.

Figure 6 shows the 20 cm (1374 MHz) pulse profile from the November observations and the 10 cm (3100 MHz) pulse profile obtained by folding and dedispersing the data with the nominal pulsar parameters and a DM of 563 cm^{-3} pc. The pulsed emission is clearly detected at 10 cm although the S/N is low. The profile appears very broad and almost sinusoidal at both frequencies. The profiles have been calibrated in flux density units, giving mean pulsed flux densities of approximately 0.25 mJy and 0.11 mJy at 20 cm and 10 cm, respectively. The upper limit on the pulsed flux density at 50 cm is about 0.5 mJy. At face value, these results imply a rather flat pulsar spectrum with spectral index $\alpha \sim -1.0$ (throughout this paper, $S_\nu \propto \nu^\alpha$). Radio observations with improved sensitivity and with contemporaneous X-ray observations will be required to explore the details of the radio pulse morphology and the phase relationship with the X-ray pulse. Distance estimates based on the observed DM are 9.4 kpc (Taylor & Cordes 1993) and 11.3 kpc (NE2001; Cordes & Lazio 2002). Given the large uncertainties inherent in DM-based distances, a reasonable estimate for the pulsar distance is 10 ± 3 kpc.
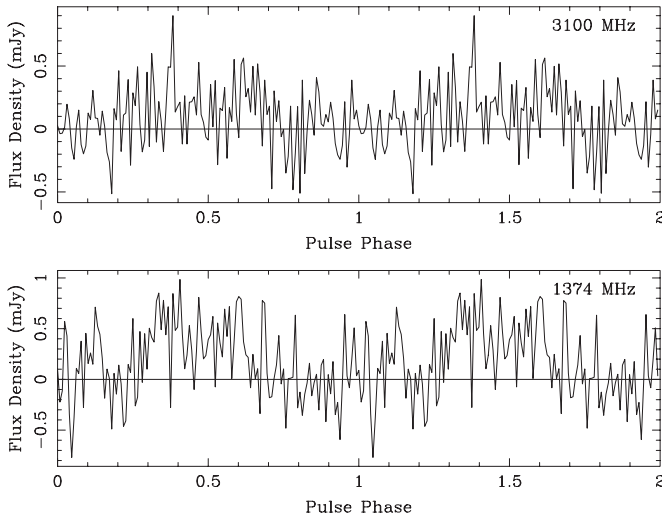
Figure 6. Radio pulse profiles at 10 cm (upper) and 20 cm (lower) folded at the predicted pulse period and dedispersed with a DM of 563 cm^{-3} pc. The pulse has been approximately centered in both plots.

2.5.2. Wind Nebula

Young PSRs are often associated with wind nebulae, usually detected in the radio and X-ray domains. We searched for the radio counterpart of the *Chandra* SNR in the archival data of the Molonglo Galactic Plane Survey at 843 MHz (MGPS-2; Murphy et al. 2007), the 2.4 GHz Parkes survey of the Southern Galactic Plane (Duncan et al. 1995), and the Parkes–MIT–NRAO (PMN) survey at 4.85 GHz (Griffith & Wright 1993; Condon et al. 1993). We found an extended MGPS-2 source, MGPS J140045−632542, located at R.A.(J2000) = 14^{h}00^{m}45^s.17, decl.(J2000) = −63°25′42″.2, 3″.5 away from the *Chandra* point-like source. The intrinsic source size of 44″.8 × 31″.2 (after deconvolution from the MOST beam size of ∼45″) is depicted in Figure 1 (left) by the dashed ellipse, which nicely matches the X-ray PWN, and thus corresponds to its radio counterpart. The 843 MHz flux density was measured to be 217.4 ± 9.4 mJy (Murphy et al. 2007). In the 4.85 GHz PMN data, we found an other cataloged source coincident with the *Chandra* SNR. According to Wright et al. (1994), PMN J1400−6325 lies at R.A.(J2000) = 14^{h}00^{m}45^s.2, decl.(J2000) = −63°25′43″. With an angular resolution of 5′ (FWHM), the source is unresolved, and features a flux density of 113 (131) ± 10 mJy, depending on the fit procedure used (see Griffith & Wright 1993; Wright et al. 1994). No significant emission is detected in the Parkes image at 2.4 GHz (Duncan et al. 1995), and we calculated a 3σ upper limit of 0.6 Jy. A power-law fit on these three radio measurements gives a spectral index α of −0.33 ± 0.05, −0.205 ± 0.008, and a flux density at 1 GHz of (0.207–0.204) ± 0.008 Jy, depending on the adopted MGPS-2 source flux. Such α index is similar to those measured in other radio PWNe (Gaensler & Slane 2006), and we can safely conclude these MGPS-2 and PMN sources are the counterparts of the X-ray wind nebula discovered with *Chandra*.

No radio shell-type structure is detected in the MGPS-2 image, even though the MOST angular resolution should allow us to separate it from the PWN. We have calculated an upper limit on the SNR surface brightness by modeling the SNR as a uniform annulus with a mean radius of 1′.15 and a width of 0′.15 (see Figure 1, right) and convolving it with the MOST beam size. The upper limit, derived by summing all the pixels within a region encompassing the FWHM of the simulated MGPS-2

shell emission, is 2.5 × 10^{-21} W m^{-2} Hz^{-1} sr^{-1} at 843 MHz, which corresponds to 2.3 × 10^{-21} W m^{-2} Hz^{-1} sr^{-1} at 1 GHz (for α = −0.5), as commonly used in studies of radio shell-type SNRs (Green 2009).

3. DISCUSSION

3.1. General Considerations

After the Crab pulsar, PSR J1400−6325 is one of the most energetic pulsars known in the Galaxy, rivaling the recently discovered PSRs associated with G12.82−0.02 and G0.9+0.1 SNRs (Gotthelf & Halpern 2009; Camilo et al. 2009). Its characteristic age τ_c of 12.7 kyr likely overestimates the true age τ, based on comparison with the SNR estimate (see below), consistent with the fact that the pulsar has not spun down significantly. We then assume in the following that $\tau \ll \tau_c$ (i.e., $P \sim P_0$ and $\dot{E} \sim \dot{E}_0$). The commonly used relations between PSR/PWN X-ray spectra (2–10 keV indices and luminosities) and the intrinsic PSR properties (Possenti et al. 2002; Gotthelf 2003; Mattana et al. 2008; Li et al. 2008), provide consistent estimates with those measured here, though with the large uncertainties inherent of such correlation studies. Amongst these relations, those between PSR/PWN X-ray luminosities and $\dot{E}$ point toward a distance to the source of 6–10 kpc, compatible with the DM-based estimate of 10 ± 3 kpc. On the one hand, the high N_H derived from the *Chandra* spectra suggests either a large source distance, or local absorption that could be undetectable in the existing large-scale H I and ^{12}CO Galactic surveys at moderate angular resolutions. Using the latest relation between optical extinction and N_H of Güver & Özel (2009), we find an extinction A$_V$ ∼ 9 toward IGR J14003−6326. Furthermore, according to the Galactic interstellar extinction map of Marshall et al. (2006), such A$_V$ along the IGR J14003−6326 line of sight corresponds to a distance of 5–8 kpc. For such a high extinction, only in the case of an overluminous core-collapse SN event (with $M_V < -17$; see Richardson 2009) would the stellar explosion of G310.6−1.6 have been visible with the naked eye ($m_V \leqslant 6$) for distances $\geqslant 5$ kpc. On the other hand, its Galactic latitude $b \sim -1°.6$ translates into a height from the Galactic plane of ∼280 pc at 10 kpc, which is much larger than the typical scale height of the Galactic molecular disk (∼55 pc; e.g., Ferrière 2001) within which core-collapse SNe are known to usually explode.[8] We also note that the Galactic longitude of G310.6−1.6 corresponds to the Crux–Scutum arm tangent, at 6–7 kpc (Vallée 2008), where much of the molecular material along this line of sight lies. In order to account for all the above-mentioned estimates with their respective uncertainties, we then adopt a distance of 7 kpc, which implies a height similar to that of the Crab nebula, and scale the distance in terms of $d_7 = d/7$ kpc.

The very small angular size of G310.6−1.6 ∼ 2′.3 = 4.7 d_7 pc already places it amongst the smallest known SNRs, and could in turn imply a very young age, similar to the recently rediscovered G1.9+0.3 SNR (Reynolds et al. 2008), and the well-known *Tycho*, *Kepler*, and Cas A SNRs. For a uniform ambient medium of density n_0 cm^{-3}, the SNR has swept up only $M_{sw} = (4\pi/3) n_0 R^3 \sim 1.3 n_0 d_7^3 M_\odot$ and thus may still be in free expansion phase. In such a case, for a typical ejected mass of $M_{ej} = 10 M_{10} M_\odot$ and an SN explosion kinetic energy of $10^{51} E_{51}$ erg, the expansion velocity

---

[8] We note that G310.6−1.6 could potentially originate from a runaway OB/Wolf-Rayet star (see, e.g., Dray et al. 2005). This scenario would explain the large height from the Galactic plane for a distance of 10 kpc.

would be $\sim 3200\,(E_{51}/M_{10})^{1/2}$ km s^{-1}, implying an age ~ 720 $d_7(M_{10}/E_{51})^{1/2}$ yr. Such a young age is also supported by the nearly circular shape of the SNR, with the PSR lying very near its geometrical center. An offset of $\lesssim 2\overset{''}{.}5$, as estimated on the *Chandra* image, implies a projected space PSR velocity of only $\lesssim 80\,d_7\tau_3^{-1}$ km s^{-1}, with $\tau = 10^3\,\tau_3$ yr, i.e., significantly smaller than the average found by Hobbs et al. (2005) for young PSRs. If we assume G310.6−1.6 has produced the same amount of ^{44}Ti as Cas A (Renaud et al. 2006), the IBIS/ISGRI upper limit on the two low-energy ^{44}Ti lines would translate into a lower limit on its age of ~ 280 yr at 7 kpc. If younger G310.6−1.6 would not have originated from one of these ^{44}Ti-rich SN explosions whose remnants (except Cas A) have been unfruitfully searched by several missions over the past decades (e.g., Renaud et al. 2004; The et al. 2006).

3.2. PWN Broadband Emission and Energetics

In order to account for the different spectral indexes measured in radio and X-ray domains (see Section 2.5 and Table 2), the PWN broadband synchrotron spectrum should exhibit a break at $\sim 3 \times 10^4$ GHz. Such frequency, if originated from synchrotron cooling of accelerated electrons inside the PWN, would correspond to an uncomfortably high magnetic field strength $B \sim 330\,\tau_3^{-2/3}$ μG. In such a case, the PWN should have appeared smaller in X-rays than in radio, in contradiction with what is shown in Figure 1. This break could instead reflect the injected electron spectrum (see, e.g., Camilo et al. 2006) or the nature of the magnetic field and of the resulting synchrotron emission (Fleishman & Bietenholz 2007). As presented in Section 2.4, the break measured at ~ 6 keV could be that expected from synchrotron cooling and, thus, provides a PWN age $\tau \sim 880\,B_{10}^{-3/2}$ yr, with $B = 10\,B_{10}$ μG. VHE observations can help further constrain the magnetic field strength inside the PWN. As reported by Chaves et al. (2008), no point-like source toward IGR J14003−6326 is detected above 5σ in the latest map of the H.E.S.S. Galactic Plane Survey, in 15 hr of effective time. This translates into an H.E.S.S. upper limit of 4% of the Crab nebula (Khélifi et al. 2008), i.e., 3×10^{-12} erg cm^{-2} s^{-1} in the 1–10 TeV energy range. In a simple one-zone leptonic scenario, the VHE emission comes from inverse-Compton scattering of VHE electrons on ambient photons (cosmic microwave background and infrared and optical Galactic fields, from dust and stars, respectively). From the ratio between the X-ray flux and the H.E.S.S. upper limit, we find that the magnetic field must be larger than 6 μG, and then, the age must be smaller than ~ 1900 yr. The corresponding maximal energy content in particles $E_{\rm p,max}$ amounts to $\sim 2.2 \times 10^{48}\,d_7^2$ erg.

PWN energetics can also provide useful insight into the source age, as young PWNe usually feature a ratio between the internal energy $E_{\rm int}$ and the PSR rotational spin-down energy $E_{\rm sd} \equiv \dot{E}\tau < 1$ (~ 0.44 for $\tau \ll$ the initial PSR spin-down time τ_0 and depends weakly on the SN density profile; see Chevalier 2005, Equation (30)). On the one hand, $E_{\rm p, max}$ thus provides a conservative limit $E_{\rm sd, max} \sim 5 \times 10^{48}\,d_7^2$ erg, which implies a maximal age of ~ 3000 yr for $\dot{E} = 5.1 \times 10^{37}$ erg s^{-1}. On the other hand, a lower limit on $E_{\rm int}$ can be obtained from equipartition arguments (Govoni & Feretti 2004; Chevalier 2005). We estimate that $E_{\rm int,min} \sim 4 \times 10^{46}\,d_7^{17/7}$ erg, i.e., $\ll \dot{E}\tau_3 = 1.6 \times 10^{48}$ erg, and a magnetic field at equipartition $B_{\rm eq} \sim 81\,d_7^{-4/14}$ μG, from the radio properties of the PWN. In case IGR J14003−6326 is at the equipartition between particles and magnetic field, its age

would then be $\ll 1$ kyr. However, H.E.S.S. has recently discovered VHE γ-ray emission toward two other young PWNe, G21.5−0.9 and Kes 75 (Djannati-Ataï et al. 2008). These observations imply magnetic fields of 10–15 μG, well below the equipartition values, and therefore support earlier suggestions (Chevalier 2005) that some young PWNe are particle dominated. If the same applies to IGR J14003−6326, $E_{\rm int}$ at the equipartition does not reflect the whole PWN energy content, and $E_{\rm int}(B) \propto B^{-3/2}$ in the particle-dominated regime. In this regime, following Chevalier (2005), the $E_{\rm int}(d, B)/\dot{E}\tau \sim 0.44$ relation, valid when $\tau \ll \tau_0$ as assumed here, would be consistent with the existence of a break measured at ~ 6 keV ($\tau \sim 880\,B_{10}^{-3/2}$ yr) for a distance of 7–8 kpc.

3.3. The Evolutionary Stage of G310.6−1.6

As discussed previously, several arguments point toward a very young composite SNR. The ratio[9] between the PWN and SNR radii is $R \approx 1/4$ and can be used to probe the parameters governing the early evolution of composite SNRs, namely E_{51}, $M_{\rm ej}$, and n_0 (van der Swaluw et al. 2001; Blondin et al. 2001), given the $\dot{E}$ measured with *RXTE*. First, n_0 and E_{51} are constrained by the faint X-ray level, and the 1 GHz upper limit, of the SNR synchrotron surface brightness. According to Berezhko & Völk (2004), such low values can only be explained by a very tenuous medium ($n_0 \lesssim 0.01$ cm^{-3}),[10] together with a sub-energetic explosion. Furthermore, using the so-called radius method of van der Swaluw & Wu (2001), the rotational energy $E_{\rm sd}$ relates to the PWN to SNR radius ratio R as $E_{\rm sd} \sim 2 \times 10^{48}\,E_{51}\,(R/0.25)^3\,(\eta_3/2)^{-3}$ erg, or $\tau \sim 1200\,E_{51}\,(R/0.25)^3\,(\eta_3/2)^{-3}$ yr, with η_3 a dimensionless parameter ranging between 1 and 3 during the early evolution phase (see their Figure 1). With the upper limit on $E_{\rm sd}$ estimated from the H.E.S.S. non detection, and the lower limit $E_{\rm int,min}$ from equipartition arguments, we infer $0.02\,d_7^{17/7}\,(\eta_3/2)^3 < E_{51} < 1\,d_7^2\,(\eta_3/2)^3$, in agreement with the weak radio and X-ray surface brightnesses of the SNR. We estimate the initial PSR period $P_0 \gtrsim 29.5$ ms (for a braking index $n = 3$), for a current period of 31.18 ms. Based on the Blondin et al. (2001) and Chevalier (2005) calculations, we then explored a wide range of E_{51}, n_0, and $M_{\rm ej}$ (the power-law index of the ejecta distribution was set to 12). For a distance of 7 kpc, if n_0 is set to 0.01 cm^{-3}, we find that only a sub-energetic ($E_{51} = 0.05$), low ejecta mass ($M_{\rm ej} = 3\,M_\odot$) SN explosion could explain the measured R. The resulting SNR age and PWN magnetic field are ~ 920 yr and ~ 10 μG, respectively. Note that the constraint on n_0 is only *qualitative*, as a quantitative estimate would require a detailed modeling of the SNR synchrotron emission, as performed by Berezhko & Völk (2004). If we relax this constraint and set n_0 to the Galactic value of 1 cm^{-3}, this would result in a larger energy of the explosion ($E_{51} = 0.4$), and a smaller SNR age ($\tau \sim 550$ yr), for the same mass of the ejecta. In this regard, knowing the nature of the SNR X-ray emission is crucial to assess the thermal flux level, and then, the surrounding density.

4. CONCLUSION

Even though some assumptions have been made in the previous estimates (e.g., constant PWN magnetic field and PSR

---

[9] The radio PWN found in the MGPS-2 data is elliptical, so that we suppose its effective size to be $\sqrt{44\overset{''}{.}8 \times 31\overset{''}{.}2}$. This yields a PWN to SNR size ratio of $\sim 37''/2\overset{'}{.}3 \sim 1/4$.

[10] This argues against a local absorption at the origin of the large $N_{\rm H}$, and distances much less than the Crux-Scutum spiral arm tangent.

spin-down power), they give valuable insight into the nature of this new Galactic composite SNR. G310.6−1.6 harbors a highly energetic 31.18 ms pulsar, PSR J1400−6325, which powers a wind nebula, both lying at the center of the host shell. All of the existing multi-wavelength observations suggest that it is a young SNR (∼1000 yr), and most likely distant (>5 kpc). However, many questions still remain to be answered. First, the distance is not very well constrained, though a large distance is favored by the dispersion measure of the radio pulse emission and by the large N_H measured with *Chandra*. High-resolution observations of the interstellar matter tracers such as H I and ^{12}CO are then warranted to assess the surrounding medium properties. Moreover, the break measured at 6 keV and the spectral softening at increasing distances in the PWN need to be confirmed, and the SNR X-ray spectrum needs to be investigated with more X-ray data. Nevertheless, G310.6−1.6 falls into the emerging class of "multi-wavelength," young ($\tau \lesssim$ a few 10^3 yr) and composite SNRs, harboring very energetic PSRs and wind nebulae shining in radio, X-rays and potentially in HE/VHE γ-rays. The list includes Kes 75 and G21.5−0.9 (Gotthelf et al. 2000; Camilo et al. 2006; Bietenholz & Bartel 2008; Djannati-Ataï et al. 2008), and more recently G0.9+0.1 (Aharonian et al. 2005a) and H.E.S.S. J1813−178 (Aharonian et al. 2005b), whose long-expected PSRs have recently been discovered (Camilo et al. 2009; Gotthelf & Halpern 2009). It is of interest to note that *Fermi*/LAT (Atwood et al. 2009) has not detected a bright source (Abdo et al. 2009a), nor pulsar (Abdo et al. 2009b, 2010) coincident with G310.6−1.6, although, at first glance, energetic PSRs should be the most easily detectable sources. However, not all of the above-mentioned young and energetic PSRs have been detected by *Fermi*. From the first *Fermi* catalog of gamma-ray PSRs, the sensitivity for a blind search of pulsed emission in the Galactic plane is conservatively taken to be 2×10^{-7} cm^{-2} s^{-1} above 100 MeV (Abdo et al. 2010). Assuming a spectrum similar to that of PSR J1833−1034 associated with G21.5−0.9, PSR J1400−6325 features a maximal efficiency $\eta = L_\gamma / \dot{E}$ of ∼1 d_7^2%. This is close to what is measured from other young PSRs (see Figure 6 of Abdo et al. 2010) and argues in favor of a fairly large distance to the source, as outlined in Section 3. Further HE/VHE observations of G310.6−1.6 will certainly provide important constraints both on the PSR gamma-ray spectrum and on the PWN magnetic field strength.

REFERENCES

Abdo, A. A., et al. (*Fermi* Collaboration) 2009a, ApJS, 183, 46
Abdo, A. A., et al. (*Fermi* Collaboration) 2009b, Science, 325, 840
Abdo, A. A., et al. (*Fermi* Collaboration) 2010, ApJS, 187, 460
Aharonian, F., et al. (H.E.S.S. Collaboration) 2005a, A&A, 432, L25
Aharonian, F., et al. (H.E.S.S. Collaboration) 2005b, Science, 307, 1938
Ahmad, I., et al. 2006, Phys. Rev. C, 74, 065803
Anders, E., & Grevesse, N. 1989, Geochim. Cosmochim. Acta, 53, 197
Atwood, W. B., et al. (*Fermi* Collaboration) 2009, ApJ, 697, 1071
Berezhko, E. G., & Völk, H. J. 2004, A&A, 427, 525
Bietenholz, M. F., & Bartel, N. 2008, MNRAS, 386, 1411
Bird, A. J., et al. 2007, ApJS, 170, 175
Blondin, J. M., Chevalier, R. A., & Frierson, D. M. 2001, ApJ, 563, 806
Bocchino, F., et al. 2005, A&A, 442, 539
Brogan, C. L., et al. 2006, ApJ, 639, L25
Camilo, F., et al. 2006, ApJ, 637, 456
Camilo, F., et al. 2009, ApJ, 700, L34
Chaves, R. C. G., et al. 2008, in AIP Conf. Proc. 1085, Proc. 4th International Meeting on High Energy Gamma-ray Astronomy, ed. F. A. Aharonian, W. Hoffmann, & F. Rieger (Melville, NY: AIP), 219
Chevalier, R. A. 2005, ApJ, 619, 839
Condon, J. J., Griffith, M. R., & Wright, A. E. 1993, AJ, 106, 1095
Cordes, J. M., & Lazio, T. J. W. 2002, arXiv:astro-ph/0207156
Djannati-Ataï, A., et al. 2008, in Proc. 30th ICRC (Mérida) 2, 823
Dray, L. M., et al. 2005, MNRAS, 364, 59
Duncan, A. R., et al. 1995, MNRAS, 277, 36
Ferrière, K. M. 2001, Rev. Mod. Phys, 73, 1031
Fleishman, G. D., & Bietenholz, M. F. 2007, MNRAS, 376, 625
Gaensler, B. M., & Slane, P. O. 2006, ARA&A, 44, 17
Gaensler, B. M., et al. 2008, ApJ, 680, L37
Garmire, G. P., Bautz, H. W., Ford, P. G., Nousek, J. A., & Ricker, Jr., G. R. 2003, Proc. SPIE, 4851, 28
Gelfand, J. D., & Gaensler, B. M. 2007, ApJ, 667, 1111
Goldwurm, A., et al. 2003, A&A, 411, L223
Gotthelf, E. V. 2003, ApJ, 591, 361
Gotthelf, E. V., & Halpern, J. P. 2009, ApJ, 700, L158
Gotthelf, E. V., et al. 2000, ApJ, 542, L37
Govoni, F., & Feretti, L. 2004, Int. J. Mod. Phys., 13, 1549
Green, D. A. 2009, Bull. Astron. Soc., India, 37, 45
Griffith, M. R., & Wright, A. E. 1993, AJ, 105, 1666
Güver, T., & Özel, F. 2009, MNRAS, 400, 2050
Hobbs, G., et al. 2005, MNRAS, 360, 974
Iyudin, A. F., et al. 1994, A&A, 284, L1
Jahoda, K., et al. 1996, Proc. SPIE, 2808, 59
Keek, S., Kuiper, L., & Hermsen, W. 2006, ATel, 810
Khélifi, B., et al. 2008, in Proc. 30th ICRC (Mérida) 2, 803
Li, X.-H., Lu, F.-J., & Li, Z. 2008, ApJ, 682, 1166
Malizia, A., et al. 2007, ApJ, 668, 81
Manchester, R. N., et al. 2001, MNRAS, 328, 17
Marshall, D. J., et al. 2006, A&A, 453, 635
Mattana, F., et al. 2008, ApJ, 694, 12
Murphy, T., et al. 2007, MNRAS, 382, 382
Possenti, A., et al. 2002, A&A, 387, 993
Prat, L., et al. 2008, MNRAS, 389, 301
Renaud, M., et al. 2004, in 5th INTEGRAL Workshop on the INTEGRAL Universe, ed. V. Schönfelder, G. Lichti, & C. Winkler (ESA SP-552; Noordwijk: ESA), 81
Renaud, M., et al. 2006, ApJ, 647, L41
Reynolds, S. P., et al. 2008, ApJ, 680, L41
Richardson, D. 2009, AJ, 137, 347
Rodriguez, J., et al. 2009, A&A, 508, 889
Safi-Harb, S., et al. 2001, ApJ, 561, 308
Slane, P., et al. 2000, ApJ, 533, L29
Taylor, J. H., & Cordes, J. M. 1993, ApJ, 411, 674
The, L.-S., et al. 2006, A&A, 450, 1037
Tomsick, J. A., et al. 2009, ApJ, 701, 811
Valinia, A., & Marshall, F. E. 1998, ApJ, 505, 134
Vallée, J. P. 2008, AJ, 135, 1301
van der Swaluw, E., & Wu, Y. 2001, ApJ, 555, L49
van der Swaluw, E., et al. 2001, A&A, 380, 309
Vink, J., et al. 2001, ApJ, 560, L79
Wilms, J., Allen, A., & McCray, R. 2000, ApJ, 542, 914
Wright, A. E., et al. 1994, ApJS, 91, 111